Research Square

Preprints are preliminary reports that have not undergone peer review.
They should not be considered conclusive, used to inform clinical practice,
or referenced by the media as validated information.

Dispersion Characteristics of Love-Type Waves in Composite Structures with Imperfect Interfaces

Juhi Baroi
Vellore Institute of Technology University
Mohammed Bilal P
mohammedbilal.p@vit.ac.in

Vellore Institute of Technology University
Pradeep Kumar Saroj
Gati Shakti Vishwavidyalaya

Article

Keywords:

Posted Date: November 23rd, 2026

DOI: https://doi.org/10.21203/rs.3.rs-11547511/v1

License: This work is licensed under a Creative Commons Attribution 4.0 International License.
Read Full License

Additional Declarations: No competing interests reported.

Dispersion Characteristics of Love-Type Waves in Composite Structures with Imperfect Interfaces

Juhi Baroi[a], Mohammed Bilal P [b*] & Pradeep Kumar Saroj[c]

[a,b]School of Advanced Sciences, Vellore Institute of Technology, Vellore, India-632004.

[c]Department of Mathematics, Gati Shakti Vishwavidyalaya, Vadodara, India-

*Corresponding author email: mohammedbilal.p@vit.ac.in

Abstract

An analytical technique is employed to study the influence of Love-type waves in a heterogeneous pre-stressed orthotropic layer sandwiched between the pre-stressed piezoelectric layer and an irregular viscous sandy (IVS) substrate under the effect of hydrostatic stress (HS). The analysis integrates a loosely bonded interface between the piezoelectric and orthotropic layers, and a parabolic-shaped irregularity is considered for the lower boundary. Using the derived dispersion relation for both electrically open and short cases (EOC/ESC), the phase velocity of the Love-type wave is studied under the effects of HS, initial stress, loose bonding, and surface irregularity thickness. Numerical results and the graphical interpretation are presented to demonstrate that the HS and initial stress significantly influence wave propagation, while bonding conditions and irregularity thickness alter dispersion characteristics. The current study findings provide critical insight for optimizing the design and performance of Surface Acoustic Wave (SAW) devices in different environments where mechanical and electrical pre-stress conditions play a crucial role.

Keywords: Prestressed Piezoelectric Material, Love-Type Wave, Dispersion Equation, Interface Mechanics, Loose Bonding, SAW Devices.

1 Introduction

The propagation of Love-type waves is a subset of surface waves and of significant importance in various fields such as engineering, electronics, seismology, geophysics, and mechanical engineering. These waves are crucial in the context of signal transmission and the improvement of surface acoustic wave (SAW) devices, which are used in filters, transducers, actuators, delay lines and sensors. The Love-type waves exploration in piezoelectric structures has gained prominence due to the sustained application of piezoelectric materials in modern technology. Jakoby and Yellekoop [1] have thoroughly examined the essential properties of Love waves in sensor devices. Du et al. [2] studied the characteristics and applications of Love wave acoustic sensors.

Piezoelectric materials are a major area of research focus due to their inherent characteristic of interaction between electric fields and mechanical fields. This property makes them highly applicable in the manufacturing, design, and advancement of SAW technology, communication systems, television broadcasting, cellular phones, and GPS-integrated SAW filters. Jiansheng Liu and Shitang He [3] have investigated the Love waves propagation in layered piezoelectric structures, while S. A. Sahu et al. [4] and P. K. Saroj et al. [5] have explained the transmission of surface waves through functionally graded piezoelectric structures. Dynamic response of acoustic wave devices in inhomogeneous media has been visualized by Sergey V. Biryukov et al. [6]. Functionally graded materials (FGMs) are composite materials derived from two or more basic materials, designed to achieve high performance in material science. Functionally graded piezoelectric materials (FGPMs) have been established to enhance the performance and operational lifespan of SAW devices. Researchers such as Li et al. [7], Liu et al. [8], and Tani et al. [9] have contributed significantly to the studies on wave transmission in FGPM and FGM.

The sandy layer, an important geological layer, is often subject to viscosity and internal friction, affecting wave propagation. P. Alam [10] studied the torsional

waves in poroelastic media sandwiched between layers of non-homogeneous dry sandy medium. A. K. Singh et al. [11] explored the behavior of shear horizontal wave propagation in a corrugated viscous sandy strip sandwiched between two elastic substrates. The challenges of wave propagation in sandy media have been discussed by S. Dey et al. [12], S. K. Tomar and J. Kaur [13].

The characteristics of the layers or the medium through which surface waves travel have a significant impact on their propagation velocity. Research has been conducted on the propagation of surface waves in an irregular stratified structure, with many authors considering irregularities of various geometries and dimensions, including rectangular and parabolic forms [14]. A. Chattopadhyay et al. [15] investigated the behavior of transversely polarized shear wave dispersion in a semi-infinite self-reinforced medium with the coating of an irregular heterogeneous self-reinforced crustal. A. K. Singh et al. [16] have visualized the propagation of Love-type waves in irregularly structured piezoelectric materials. Initial stress significantly influences wave propagation in various elastic media. J. Du et al. [17] and P.Singh et al. [18] investigated the wave dynamics of Love wave in a prestressed medium.

Although significant research has been conducted on Love-type waves across various media, a significant gap persists in understanding their propagation within complex structures, specifically those involving a prestressed heterogeneous orthotropic layer sandwiched between a prestressed piezoelectric layer and an IVS substrate. Previous studies have largely focused on individual aspects such as piezoelectric materials, functionally graded materials, and sandy media. However, the combined effects of these elements alongside factors like loose bonding, irregularity, material gradient coefficients, initial stress, and HS remain underexplored. This research is motivated by the potential to enhance the design and efficiency of surface acoustic wave (SAW) devices, which are pivotal in modern communication and signal processing technologies. By delving into these complex interactions,

our study aims to fill this gap, offering novel insights that could lead to the development of more robust and efficient SAW devices. The comprehensive approach adopted in this research not only addresses the existing gaps but also provides a deeper understanding of wave behavior in layered media, contributing significantly to the advancement of material science and engineering.

The current study aims to analyze the propagation of Love-type surface waves in a prestressed heterogeneous orthotropic layer sandwiched between a prestressed piezoelectric layer and an IVS substrate with HS. The dispersion equation for the considered configuration has been obtained in determinant form for electrically open and short conditions. Dispersion curves are plotted to specify the dependence of phase velocity and wave numbers on the constants and the elastic modulus. This study addresses the effects of loose bonding, material gradient coefficient, irregularity, initial stress, and HS on the phase velocity and wave number of Love-type waves.

2 Fundamental assumption

3 Fundamental assumption

A single real bonding parameter was introduced by G. Murty [19] and G. S. Murty [20], where numerical values correspond to varying levels of bonding between two substrates. In his analysis, he demonstrated that an ideally smooth interface exhibits acoustic behavior associated with a bonding parameter of 0, whereas a fully bonded interface corresponds to ∞. Two core assumptions form the basis of the study conducted by Murty. The primary assumption states that a loosely bonded interface between two elastic substrates preserves boundary continuity. The second assumes that the slip at the interface maintains a direct proportionality

with the localized shear stress represented as

$$\text{Shearing stress} = B \times \text{Slip} \tag{1}$$

Here, the proportionally constant B represents the bonding strength. A vanishing value of B corresponds to a perfectly smooth interface, while B represents a fully welded interface at an infinitely large value. Intermediate values of B indicate a partially bonded interface.

Further, dimensional analysis of eq. (1) suggests that B cannot be a purely real number. To address this, a newly introduced real parameter Ω in the shearing stress as

$$\text{Shearing stress} = ikN\zeta \left(v_z^{(p)} - v_z^{(o)}\right) \tag{2}$$

where $\zeta = \frac{c}{\beta_1}\frac{\Omega}{1-\Omega}$ is a purely real number, N denote rigidity for second layer, and $v_z^{(p)}, v_z^{(o)}$ represent the displacement components of the first and second layers, respectively.

Consequently, the shearing stress equation transforms into

$$\text{Shearing stress} = ikN\frac{c}{\beta_1}\frac{\Omega}{1-\Omega}\left(v_z^{(p)} - v_z^{(o)}\right) \tag{3}$$

Thus, when $\Omega = 0$, the interface behaves as an ideally smooth boundary, whereas for $\Omega = 1$, the shearing stress becomes infinitely large, signifying a fully welded interface.

4 Framework of the problem

A structure is considered, comprising an orthotropic layer of uniform depth $-h_1$ sandwiched between a uniformly thick pre-stressed piezoelectric layer $-h_2-h_1$ and a viscous sandy substrate subjected to HS. The substrate exhibits a parabolic-type irregularity with a span of s and a depth of H, as illustrated in figure 1.

Let us define the Cartesian coordinate system $O-xyz$, where the x-axis represents the path of wave transmission, the y-axis is directed along the polarization of the

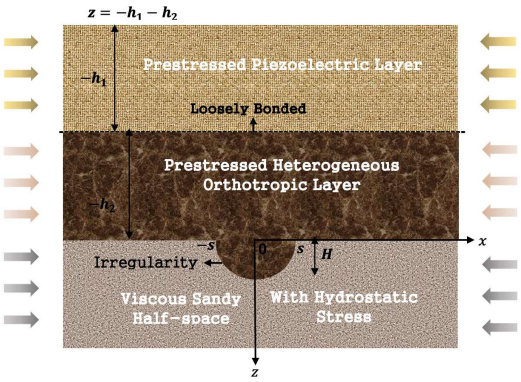


Figure 1: Geometric Structure

piezoelectric layer and perpendicular to the $x - z$ plane. The coordinate origin is located at the midpoint of the irregularity.

The equation of the irregular interface of viscous sandy substrate under HS is given by

$$z = \varepsilon_1 h(x) \tag{4}$$

Where,

$$h(x) = \begin{cases} 0 & \text{for } -s \geq x \geq s \\ \frac{2\left(s^2 - x^2\right)}{s} & \text{for } -s < x < s \end{cases} \tag{5}$$

And ε_1 is a small positive number such that $\varepsilon_1 = \frac{H}{2s} \ll 1$.

Since Love-type wave propagation is considered for the structure, without loss of generality, we assume that the wave propagates along the x-axis, allowing the mechanical displacement component and electrical potential function to be expressed in the following form.

$$v_x = v_y = 0, \quad v_z = v_z(x, z, t), \quad \phi_1 = \phi_1(x, z, t) \tag{6}$$

5 Dynamics of the upper pre-stressed piezoelectric layer

The generalized motion equations for piezoelectric material are given as

$$\left.\begin{aligned} \alpha_{ij,j} &= \rho^{(F)}\ddot{u}_{Fi} \\ \beta_{i,i} &= 0 \end{aligned}\right\} \tag{7}$$

Here, the comma denotes differentiation with respect to spatial coordinates, and the dot signifies differentiation of time dependent (t) and $u_F, \rho^{(F)}$ denote the mechanical displacement and the material density, respectively. The constitutive equation for the upper transversely isotropic piezoelectric medium can be represented as

$$\left.\begin{aligned} \alpha_x &= e_{11}Q_x + e_{12}Q_y + e_{13}Q_z - g_{31}A_z \\ \alpha_y &= e_{12}Q_x + e_{11}Q_y + e_{13}Q_z - g_{31}A_z \\ \alpha_z &= e_{13}Q_x + e_{13}Q_y + e_{33}Q_z - g_{31}A_z \\ \varphi_{yz} &= e_{44}Q_{yz} - g_{15}A_y \\ \varphi_{zx} &= e_{44}Q_{zx} - g_{15}A_x \\ \varphi_{xy} &= \frac{e_{11} - e_{12}}{2}Q_{xy} \\ \beta_x &= g_{15}Q_{zx} + \kappa_{11}A_x \\ \beta_y &= g_{15}Q_{yz} + \kappa_{11}A_y \\ \beta_z &= g_{31}Q_x + g_{31}Q_y + g_{31}Q_z + \kappa_{33}A_z \end{aligned}\right\} \tag{8}$$

Here, the parameter g_{ij} (piezoelectric constant), e_{ij} (elastic constant), and κ_{ij} (dielectric constant) for $i, j = 1, 2, ..., 6$ are dependent on x, and can be expressed as $g_{ij} \equiv g_{ij}(x), e_{ij} \equiv e_{ij}(x), \kappa_{ij} \equiv \kappa_{ij}(x)$.

For the pre-stressed piezoelectric layer, the motion equation, which is known as Gauss' law of electrostatics under charge-free conditions, is given as (Z.Wang and

F. Shang [21])

$$\alpha_{ij,j} + \left(u_{i,k}P_{kj}\right)_{i,j} = \rho_{pi}\ddot{u} \tag{9}$$

$$\beta_{i,j} + \left(u_{i,j}\beta_j^0\right)_i = 0 \tag{10}$$

Where P_{kj} signifies the initial stress and β_j^0 corresponds to the initial electric displacement. The governing equations describe the motion of Love-type waves in the prestressed piezoelectric layer.

$$e_{44}^{(p)}\frac{\partial^2 v_z^{(p)}}{\partial x^2} + \left(P_1 + e_{44}^{(p)}\right)\frac{\partial^2 v_z^{(p)}}{\partial z^2} + g_{15}^{(p)}\left(\frac{\partial^2 \phi_1^{(p)}}{\partial x^2} + \frac{\partial^2 \phi_1^{(p)}}{\partial z^2}\right) = \rho^{(p)}\frac{\partial^2 v_z^{(p)}}{\partial t^2} \tag{11}$$

$$g_{15}^{(p)}\left(\frac{\partial^2 v_z^{(p)}}{\partial x^2} + \frac{\partial^2 v_z^{(p)}}{\partial z^2}\right) - \kappa_{11}^{(p)}\left(\frac{\partial^2 \phi_1^{(p)}}{\partial x^2} + \frac{\partial^2 \phi_1^{(p)}}{\partial z^2}\right) = 0 \tag{12}$$

Where $\phi^{(p)}, v_z^{(p)}, P_1$ are electrical potential, mechanical displacement and initial stress, respectively and $\kappa_{11}^{(p)}$, $g_{15}^{(p)}$ and $e_{44}^{(p)}$ represents the dielectric, piezoelectric and elastic constants, respectively for the piezoelectric layer. Now, we assume the solutions of eqs.(11),(12) are as follows

$$\begin{aligned} v_z^{(p)}(x,z,t) &= V_z^{(p)}(z)e^{ik(x-ct)} \\ \phi_1^{(p)}(x,z,t) &= \psi^{(p)}(z)e^{ik(x-ct)} \end{aligned} \tag{13}$$

Where $k = 2\pi/\lambda$ is the wave number (λ is the wavelength) and c is the phase velocity. Using eqs.(13) in eqs.(11),(12), then the obtained ordinary differential equations are given as

$$e_{44}^{(p)}V_z^{(p)\prime\prime} + \left(P_1 + e_{44}^{(p)}\right)\left(V_z^{(p)}\right) + g_{15}^{(p)}\left(\psi^{(p)\prime\prime} - k^2\psi^{(p)}\right) = \rho^{(p)}V_z^{(p)}(-kc)^2 \tag{14}$$

$$g_{15}^{(p)}\left(V_z^{(p)\prime\prime} - k^2 V_z^{(p)}\right) - \kappa_{11}^{(p)}\left(\psi^{(p)\prime\prime} - k^2\psi^{(p)}\right) = 0 \tag{15}$$

Now, eq. (15) can be written as

$$\left(\psi^{(p)\prime\prime} - k^2\psi^{(p)}\right) = \frac{g_{15}^{(p)}}{\kappa_{11}^{(p)}}\left(V_z^{(p)\prime\prime} - k^2 V_z^{(p)}\right) \tag{16}$$

Solving eqs(14),(16) then we obtain

$$V_z^{(p)\prime\prime} - k^2 n^2 V_z^{(p)} = 0 \tag{17}$$

Where

$$n = \sqrt{\frac{\frac{P_1}{\rho^{(p)}} - \left(\frac{kc}{k}\right)^2}{\frac{e_{44}^{(p)}\kappa_{11}^{(p)} + \left(g_{15}^{(p)}\right)^2}{\rho^{(p)}}} + 1}$$

Thus, the general solution to eq.(17) can be expressed as follows

$$v_z^{(p)}(x,z,t) = \left(D_1 e^{knz} + D_2 e^{-knz}\right) e^{ik(x-ct)} \tag{18}$$

It can be observed that

$$\psi^{(p)}(\mathrm{z}) = \frac{g_{15}^{(p)}}{\kappa_{11}^{(p)}} V_z^{(p)}(\mathrm{z}) \tag{19}$$

Solving eq (15), we get

$$\psi^{(p)''} - k^2 \psi^{(p)} = 0 \tag{20}$$

Hence, the solution of the eq.(20) is as follows

$$\psi^{(p)}(\mathrm{z}) = D_3 e^{kz} + D_4 e^{-kz} \tag{21}$$

Taking the eqs. (19),(21) in eq. (13), we get the complete solution of $\phi_1^{(p)}(x)$ is given by

$$\phi_1^{(p)}(x,z,t) = \left(D_3 e^{kz} + D_4 e^{-kz} + \frac{g_{15}^{(p)}}{\kappa_{11}^{(p)}}\left(D_1 e^{knz} + D_2 e^{-knz}\right)\right) e^{ik(x-ct)}. \tag{22}$$

6 Dynamics of intermediate prestressed heterogeneous orthotropic layer

The basic relation between strain and stress for the upper heterogeneous orthotropic layer is assumed as

$$\begin{bmatrix} \varpi_{11} \\ \varpi_{22} \\ \varpi_{33} \\ \varpi_{23} \\ \varpi_{13} \\ \varpi_{12} \end{bmatrix} = \begin{bmatrix} B_{11} & B_{12} & B_{13} & 0 & 0 & 0 \\ B_{12} & B_{22} & A_{23} & 0 & 0 & 0 \\ B_{13} & B_{23} & B_{33} & 0 & 0 & 0 \\ 0 & 0 & 0 & 2Q & 0 & 0 \\ 0 & 0 & 0 & 0 & 2R & 0 \\ 0 & 0 & 0 & 0 & 0 & 2N \end{bmatrix} \begin{bmatrix} \eta_{11} \\ \eta_{22} \\ \eta_{33} \\ \eta_{23} \\ \eta_{13} \\ \eta_{12} \end{bmatrix} \tag{23}$$

Where σ_{ij} is the stress components, $B_{ij}(i,j = 1,2,3)$ and N, Q, R are elastic constants and η_{ij} are strain components.

The non-vanishing strain-displacement relation is obtained as

$$\eta_{23} = \frac{1}{2}\frac{\partial v_z^{(o)}}{\partial z}, \eta_{12} = \frac{1}{2}\frac{\partial v_z^{(o)}}{\partial x} \tag{24}$$

Using eq. (6) and eq. (24), we have a non-vanishing stress component

$$\varpi_{23} = 2Q\eta_{23} = Q\frac{\partial v_z^{(o)}}{\partial z}, \varpi_{12} = 2N\eta_{12} = N\frac{\partial v_z^{(o)}}{\partial x} \tag{25}$$

The angular displacement vector for Love wave propagation is given by

$$\omega_z = \frac{1}{2}\frac{\partial v_z^{(o)}}{\partial x} \tag{26}$$

Now, the heterogeneity is considered for the intermediate prestressed heterogeneous orthotropic layer in the following form

$$\begin{aligned} &Q = Q_2(1+\sin\alpha z), N = N_2(1+\sin\alpha z), \\ &\rho^{(o)'} = \rho^{(o)}(1+\sin\alpha z), P = P_2(1+\sin\alpha z) \end{aligned} \tag{27}$$

Where α and P_2 denote the heterogeneity parameter and initial stress, respectively. Given of eq. (6), The only non-zero equation of motion for an intermediate prestressed heterogeneous orthotropic layer is obtained as

$$\frac{\partial \varpi_{12}}{\partial x} + \frac{\partial \varpi_{23}}{\partial z} - P\frac{\partial \omega_z}{\partial x} = \rho^{(o)'}\frac{\partial^2 v_z^{(o)}}{\partial t^2} \tag{28}$$

Where $\rho^{(o)'}$ denotes the density of the layer.

Therefore, in terms of the displacement components, the equation of motion for the intermediate pre-stressed heterogeneous orthotropic layer is given by eqs. (6), (24), (25), (26), and (27). Substituting these into eq.(28), we obtain:

$$\frac{\partial^2 v_z^{(o)}}{\partial z^2} + \frac{\alpha\cos(\alpha z)}{1+\sin(\alpha z)}\frac{\partial v_z^{(o)}}{\partial z} + \left(\frac{2N_2 - P_2}{2Q_2}\right)\frac{\partial^2 v_z^{(o)}}{\partial x^2} = \frac{1}{\beta_1^2}\frac{\partial^2 v_z^{(o)}}{\partial t^2} \tag{29}$$

Where $I = \frac{2N_2 - P_2}{2Q_2}$, $\beta_1 = \sqrt{\frac{Q_2}{\rho^{(o)}}}$ is named as shear wave velocity The solution of eq.(29) may be assumed in the following form

$$v_z^{(o)}(x,z,t) = V_z^{(o)}(\mathrm{z})e^{ik(x-ct)} \tag{30}$$

Substituting eq. (30) into eq. (29), the resulting second-order differential equation is obtained as:

$$\frac{d^2V_z^{(o)}}{dz^2} + \frac{\alpha\cos(\alpha z)}{1+\sin\alpha z}\frac{dV_z^{(o)}}{dz} + k^2\left(\frac{c^2}{\beta_1^2} + I\right)V_z^{(o)} = 0 \tag{31}$$

Where $I = \frac{P_2 - 2N_2}{2M_2}$, considering $V_z^{(o)}(z) = \frac{\varphi(z)}{\sqrt{1+\sin\alpha z}}$ in the above equation to eliminate the first-order derivative term, then we obtain

$$\frac{d^2\varphi}{dz^2} + \delta^2\varphi = 0 \tag{32}$$

Where

$$\delta = \sqrt{k^2\left(\frac{\alpha^2}{4k^2} + \frac{c^2}{\beta_1^2} + I\right)}$$

Then the obtained solution of eq.(32) is given in the following form

$$V_z^{(o)}(z) = \frac{(\mathrm{A}_1\sin\delta z + B_1\cos\delta z)}{\sqrt{1+\sin\alpha z}} \tag{33}$$

Hence, the derived solution for the intermediate pre-stressed heterogeneous orthotropic layer is expressed as follows

$$v_z^{(o)}(x,z,t) = \frac{(A_1\sin\delta z + B_1\cos\delta z)}{\sqrt{1+\sin\alpha z}}e^{ik(x-ct)} \tag{34}$$

7 Dynamics of lower viscous sandy substrate with HS

The fundamental relationship between rigidity (μ), Poission's ratio (v) and Young's modulus (E) for an elastic body is expressed as $E\mu^{-1} = 2+2v$. However, in the case of a sandy layer, this relation changes to $E\mu^{-1} > 2+2v$ as a consequence of particle slippage. By introducing the sandy parameter ($\omega > 1$) leads to a transformation of the inequality into $E\mu^{-1} = 2\omega(1+v)$. Further, incorporating generalized Lame's constant into the relation $E\mu^{-1} = 2\omega(1+v)$, we obtain $\Lambda = Ev/\omega(1+v)(1-2v)$. In the account of viscous sandy layer, the rigidity μ is replaced by $\bar{\mu}_3 = \left(\mu_3 + \mu_3'\frac{\partial}{\partial t}\right)$,

where μ_3 represents the rigidity of the layer, and μ_3' denotes internal friction. The fundamental wave equation in terms of displacement is then given by

$$\partial_j \alpha_{ij} + p_i = \rho \partial_{tt} V_i \tag{35}$$

Where $p_i, \rho, V_i, \alpha_{ij}$ denote the force exerted per unit volume within the body, density, displacement components and components of stress, respectively.

In view of eq. (6) in eq. (35) we have the following non-vanishing equation of motion

$$\partial_x \alpha_{xy} + \partial_x \alpha_{zy} + p_y = \rho \partial_{tt} v_z \tag{36}$$

The propagation of Love-type waves in the lower viscous sandy substrate under HS is governed by the following equations of motion.

$$\bar{\mu}_2 \left(\omega \frac{\partial^2 v_z^{(s)}}{\partial x^2} + \frac{\partial^2 v_z^{(s)}}{\partial z^2} - P_3 \Delta^2 v_z^{(s)} \right) = \rho^{(s)} \frac{\partial^2 v_z^{(s)}}{\partial t^2} \tag{37}$$

Where P_3 is the HS, $v_z^{(s)}, \rho^{(s)}$ is the mechanical displacement and density of the layer. Moreover, in eq. (37), we obtain

$$\Delta^2 = \frac{\partial^2}{\partial x^2} + \frac{\partial^2}{\partial z^2}$$

Assuming a specific form of the wave solution, to solve the eq. (37)

$$v_z^{(s)}(x, z, t) = V_z^{(s)}(z) e^{ik(x - ct)} \tag{38}$$

Then, substituting the assumed wave solution into eq. (37), we derive the following ordinary differential equation

$$V_z^{(s)''} + m^2 V_z^{(s)} = 0 \tag{39}$$

Where

$$m = \sqrt{\frac{((P_3 - \omega)k^2)\mu_3 + ((\omega - P_3)ik^3 c)\mu_3' + k^2 c^2 \rho^{(v)}}{\mu_3(1 - P_3) + \mu_3'((P_3 - 1)ikc)}}$$

The solution of eq. (39) is given as

$$V_z^{(s)} = C_1 e^{mz} + C_2 e^{-mz} \tag{40}$$

In view of eq. (38) and (40), we have

$$v_z^{(s)}(x,z,t) = (C_1 e^{mz} + C_2 e^{-mz}) e^{ik(x-ct)} \tag{41}$$

Where C_1 and C_2 are arbitrary constants.
In light of the condition $\lim v_z^{(s)} = 0$, when $z \to \infty$. Then, the solution of viscous sandy substrate in the presence of HS is given by

$$v_z^{(s)}(x,z,t) = C_2 e^{-mz} e^{ik(x-ct)} \tag{42}$$

8 Boundary conditions

A stress-free condition is maintained on the upper surface of the prestressed piezoelectric layer at $z = h_0 = -h_1 - h_2$ i.e.

$$(\omega_{zy})_1 (x, h_0, t) = 0 \tag{43}$$

Where

$$(\varpi_{zy})_1 = e_{44}^{(p)} \left(\frac{\partial v_z^{(p)}}{\partial z} \right) + g_{15}^{(p)} \left(\frac{\partial \phi_1^{(p)}}{\partial z} \right)$$

The electrical boundary conditions at $z = h_0 = -h_2 - h_1$ are considered , while the surface is assumed to be traction-free.

$$\phi_1^{(p)} (x, h_0, t) = 0 \text{ (Electrical short condition)} \tag{44}$$

$$(\beta_z)_1 (x, h_0, t) = 0 \text{ (Electrical open condition)} \tag{45}$$

Where

$$(\beta_z)_1 = g_{15}^{(p)} \left(\frac{\partial v_z^{(p)}}{\partial z} \right) - \kappa_{11}^{(p)} \left(\frac{\partial \phi_1^{(p)}}{\partial z} \right)$$

At the interface $z = -h_2$, the stress and displacement continuity conditions between the pre-stressed piezoelectric layer and heterogeneous orthotropic layer give the following expression

$$(\varpi_{zy})_1 (x, -h_2, t) = (\varpi_{zy})_2 (x, -h_2, t) \tag{46}$$

$$\phi_1^{(p)} (x, -h_2, t) = 0 \tag{47}$$

$$(\varpi_{zy})_1 (1 - \Omega) = ikN\Omega \frac{c}{\beta_1} \left(v_z^{(p)} - v_z^{(o)} \right) \tag{48}$$

Where

$$(\varpi_{zy})_2 = M_2 \frac{\partial v_z^{(o)}}{\partial z}, N = N_2(1 + \sin \alpha z)$$

and Ω represents the bonding parameter at the interface between the prestressed piezoelectric layer and the prestressed heterogeneous orthotropic layer.

At the interface $z = \varepsilon_1 h(x)$, the stress and displacement continuity conditions between the heterogeneous orthotropic layer and an IVS substrate subjected to HS, provide the following relation

$$v_z^{(o)} (x, \varepsilon_1 h(x), t) = v_z^{(s)} (x, \varepsilon_1 h(x), t) \tag{49}$$

$$(\varpi_{zy})_2 = (\varpi_{zy})_3 \tag{50}$$

Where

$$(\varpi_{zy})_3 = \bar{\mu}_3 \frac{\partial v_z^{(s)}}{\partial z}$$

$$\left(e_{44}^{(p)} + \frac{\left(g_{15}^{(p)} \right)^2}{\kappa_{11}^{(p)}} \right) kn \left(D_1 e^{knh_0} - D_2 e^{-knh_0} \right) + g_{15}^{(p)} k \left(D_3 e^{kh_0} - D_4 e^{-kh_0} \right) = 0 \tag{51}$$

$$\frac{g_{15}^{(p)}}{\kappa_{11}^{(p)}} \left(D_1 e^{knh_0} + D_2 e^{-knh_0} \right) + D_3 e^{kh_0} + D_4 e^{-kh_0} = 0 \tag{52}$$

$$\kappa_{11}^{(p)} k \left(D_3 e^{kh_0} - D_4 e^{-kh_0} \right) = 0 \tag{53}$$

$$\left(e_{44}^{(p)} + \frac{\left(g_{15}^{(p)} \right)^2}{\kappa_{11}^{(p)}} \right) kn \left(D_1 e^{-knh_2} - D_2 e^{knh_2} \right) + g_{15}^{(p)} k \left(D_3 e^{-kh_2} - D_4 e^{kh_2} \right)$$
$$- A_1 \left(\frac{\delta \cos(\delta h_2)}{\sqrt{1 - \sin(\alpha h_2)}} + \frac{\alpha \sin(\delta h_2) \cos(\alpha h_2)}{2(1 - \sin(\alpha h_2))^{3/2}} \right) M_2 (1 - \sin(\alpha h_2)) \tag{54}$$
$$- B_1 \left(- \frac{\alpha \cos(\delta h_2) \cos(\alpha h_2)}{2(1 - \sin(\alpha h_2))^{3/2}} + \frac{\delta \sin(\delta h_2)}{\sqrt{1 - \sin(\alpha h_2)}} \right) M_2 (1 - \sin(\alpha h_2)) = 0$$

$$\frac{g_{15}^{(p)}}{\kappa_{11}^{(p)}} \left(D_1 e^{-knh_2} + D_2 e^{knh_2} \right) + D_3 e^{-kh_2} + D_4 e^{kh_2} = 0 \tag{55}$$

$$D_1 \left(\left((1 - \Omega) \left(e_{44}^{(p)} + \frac{\left(g_{15}^{(p)} \right)^2}{\kappa_{11}^{(p)}} \right) kn - ikN\Omega \frac{c}{\beta_1} \right) e^{-knh_2} \right)$$
$$- D_2 \left(\left((1 - \Omega) \left(e_{44}^{(p)} + \frac{\left(g_{15}^{(p)} \right)^2}{\kappa_{11}^{(p)}} \right) kn + ikN\Omega \frac{c}{\beta_1} \right) e^{knh_2} \right)$$
$$+ (1 - \Omega) g_{15}^{(p)} k \left(D_3 e^{-kh_2} - D_4 e^{kh_2} \right) - ikN\Omega \frac{c}{\beta_1} \left(\frac{-A_1 \sin(\delta h_2) + B_1 \cos(\delta h_2)}{\sqrt{1 - \sin(\alpha h_2)}} \right) = 0 \tag{56}$$

$$\frac{A_1 \sin(\delta \varepsilon_1 h(x)) + B_1 \cos(\delta \varepsilon_1 h(x))}{\sqrt{1 + \sin(\alpha \varepsilon_1 h(x))}} - C_2 e^{-m\varepsilon_1 h(x)} = 0 \tag{57}$$

$$A_1 \left(M_2 \delta \cos(\delta \varepsilon_1 h(x)) \sqrt{1 + \sin(\alpha \varepsilon_1 h(x))} - \frac{M_2 \alpha \sin(\delta \varepsilon_1 h(x)) \cos(\alpha \varepsilon_1 h(x))}{2\sqrt{1 + \sin(\alpha \varepsilon_1 h(x)))}} \right)$$
$$+ B_1 \left(- M_2 \delta \sin(\delta \varepsilon_1 h(x)) \sqrt{1 + \sin(\alpha \varepsilon_1 h(x))} - \frac{M_2 \alpha \cos(\delta \varepsilon_1 h(x)) \cos(\alpha \varepsilon_1 h(x))}{2\sqrt{1 + \sin(\alpha \varepsilon_1 h(x)))}} \right)$$
$$- C_2 m e^{-m\varepsilon_1 h(x)} (\mu_3 - i\mu_3' kc) = 0 \tag{58}$$

9 Dispersion equation

In this analytical study, we investigate the dispersion relation of Love-type waves propagating in a heterogeneous pre-stressed orthotropic layer, interposed between a pre-stressed piezoelectric layer and an IVS substrate. The interaction among

these layers is analyzed under HS, with a particular emphasis on the effect of a loose bonding interface between the upper piezoelectric layer and the orthotropic medium. The dispersion relation is formulated for both electrically open and short cases, enabling a comprehensive understanding of wave propagation characteristics. In the electrically open case (EOC), the boundary conditions allow the electric potential to remain free, leading to distinct phase velocity responses influenced by the piezoelectric effect and the prevailing stress state. Conversely, in the electrically short case (ESC), the electric field is effectively shorted, modifying the energy coupling between the layers and subsequently altering the wave speed.

9.1 Electrically open case (EOC)

Considering all the boundary conditions from equations (51) to (58), except for (52), we form a determinant matrix using the coefficients of the arbitrary constants. This leads to the following equation:

$$|P_{ij}| = 0 \tag{59}$$

Here, $i, j = 1, 2, \ldots, 7$, and the coefficients P_{ij} are given in Appendix A.

9.2 Electrically short case (ESC)

In this case, we consider all the boundary conditions from eqs. (51) to (58), except for (52). By forming a determinant matrix with the coefficients of the arbitrary constants, we obtain the following equation:

$$|Q_{ij}| = 0 \tag{60}$$

Where $i, j = 1, 2, \ldots, 7$, and Q_{ij} values are given in Appendix A.

10 Numerical Results and Discussions

We conduct numerical examples and visual representations of the derived dispersion relation to examine the effects of various influencing parameters on the attenuation characteristics and the phase velocity of Love-type waves. The parameters considered in this study include the heterogeneity parameter, sandiness parameter, internal friction, initial stress parameters, HS parameters, bonding parameter, and the irregularity span and depth parameters. For the numerical examples and visual representations, the following material constants have been considered:

1. Prestressed piezoelectric layer [22]

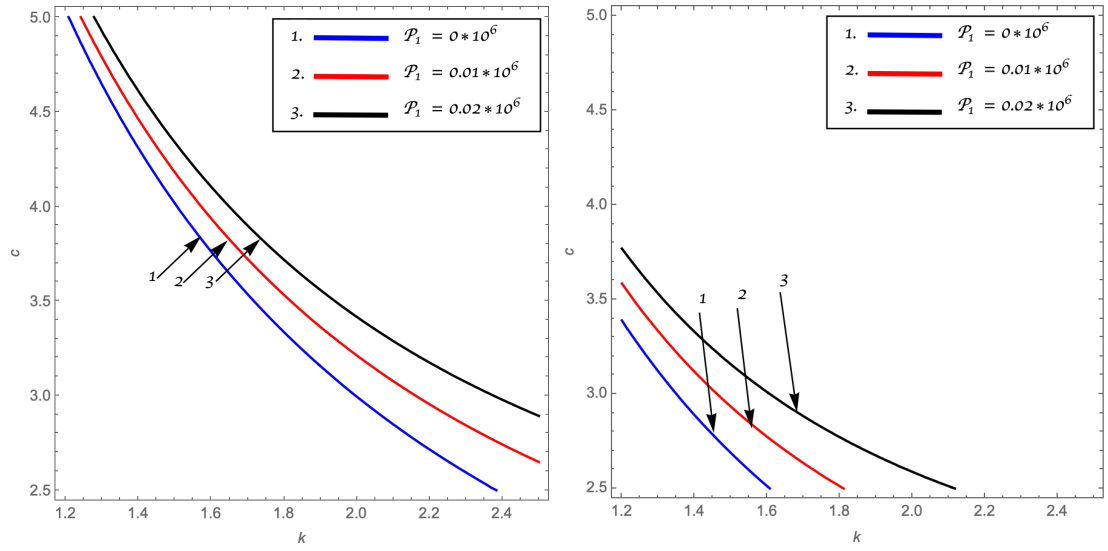
$$e_{44}^{(p)} = 27.1\ GPa, \quad g_{15}^{(p)} = 4.6\ C.m^{-2}, \quad \kappa_{11}^{(p)} = 3.6\ nF.m^{-1}, \quad \rho^{(p)} = 7800 kg.m^{-3}$$

2. Prestressed heterogeneous orthotropic layer [23]

$$M_2 = 5.82 \times 10^{10}\ N/m^2, \quad N_2 = 3.99 \times 10^{10}\ N/m^2, \quad \rho^{(o)} = 4500\ kg/m^3$$

3. Viscous sandy substrate with HS [24]

$$\mu_3 = 3.23 \times 10^{10}\ N/m^2, \quad \rho^{(s)} = 2802\ kg/m^3$$

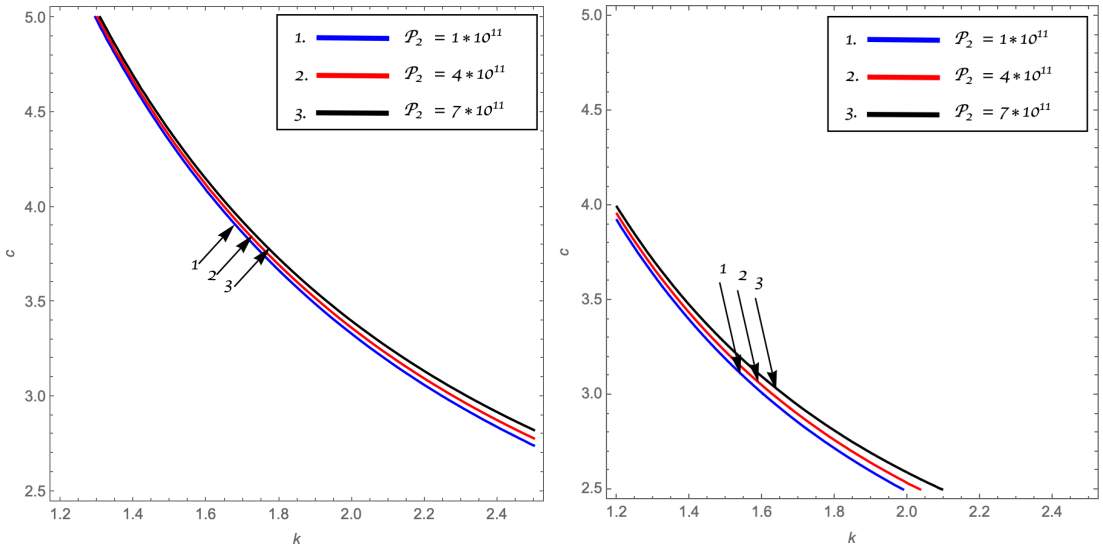


(a) (b)

Fig 2: Variation of Phase velocity (c) vs wave number (k) for the various values of initial stress (P_1),(a) electrically open case (EOC), (b) electrically short case (ESC).

Table 1: Comparison of initial stress P_1 on phase velocity c at $k = 1.4$

P_1	c (EOC)	$\Delta\%$ (EOC)	c (ESC)	$\Delta\%$ (ESC)
0	4.310	–	2.888	–
0.01×10^6	4.462	+3.53%	3.117	+7.93%
0.02×10^6	4.611	+6.99%	3.329	+15.27%

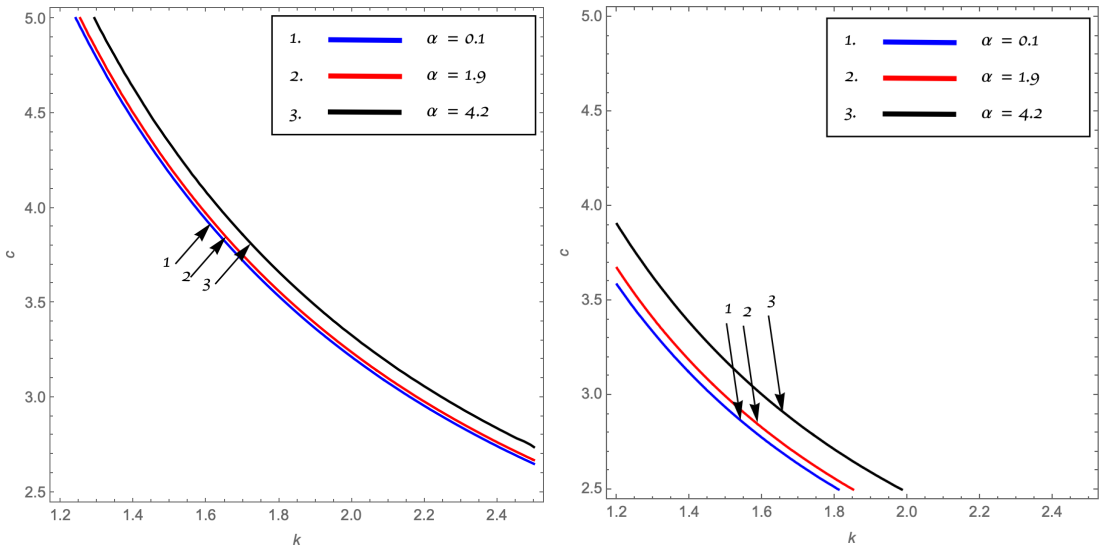


(a) (b)

Fig 3: Variation of Phase velocity (c) vs wave number (k) for the various values of initial stress (P_2),(a) electrically open case (EOC)(b) electrically short case (ESC).

Table 2: Comparison of initial stress P_2 on phase velocity c at $k = 1.4$

P_2	c (EOC)	Δ% (EOC)	c (ESC)	Δ% (ESC)
1×10^{11}	4.641	–	3.394	–
4×10^{11}	4.666	+0.54%	3.431	+1.09%
7×10^{11}	4.693	+1.12%	3.473	+2.33%

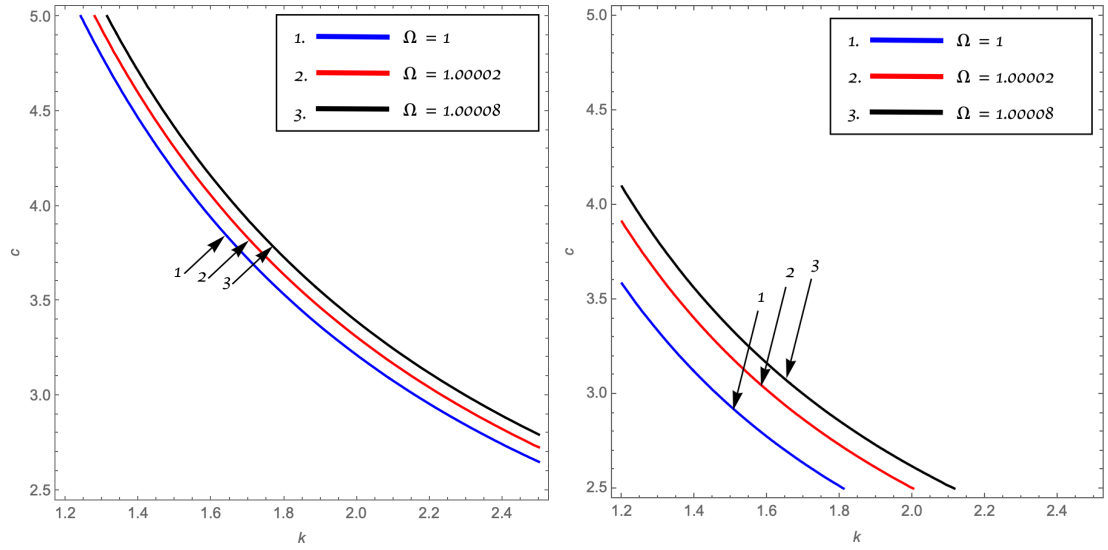


(a) (b)

Fig 4: Variation of Phase velocity (c) vs wave number (k) for the various values of heterogeneity parameter (α), (a) electrically open case (EOC) (b) electrically short case (ESC).

Table 3: Comparison of heterogeneity parameter α on phase velocity c at $k = 1.4$

α	c (EOC)	Δ% (EOC)	c (ESC)	Δ% (ESC)
0.1	4.462	–	3.117	–
1.9	4.499	+0.83%	3.181	+2.05%
4.2	4.634	+3.85%	3.383	+8.53%

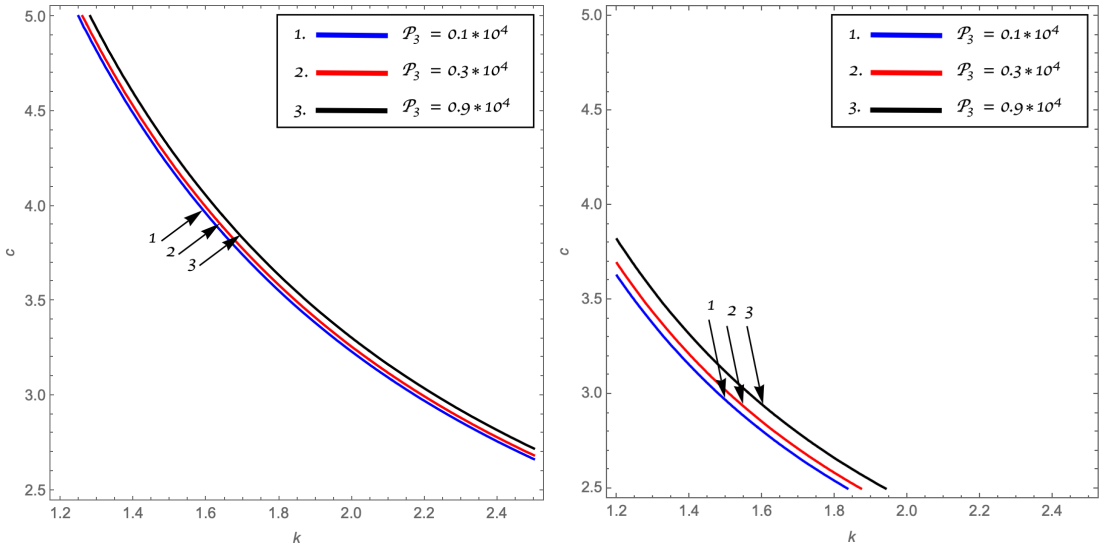


(a) (b)

Fig 5: Variation of Phase velocity (c) vs wave number (k) for the various values of bonding parameter (Ω) between the prestressed piezoelectric layer and prestressed heterogeneous orthotropic layer, (a) electrically open case (EOC) (b) electrically short case (ESC).

Table 4: Comparison of bonding parameter Ω on phase velocity c at $k = 1.4$

Ω	c (EOC)	Δ% (EOC)	c (ESC)	Δ% (ESC)
1	4.462	–	3.117	–
1.00002	4.594	+2.96%	3.399	+9.05%
1.00008	4.710	+5.56%	3.558	+14.15%

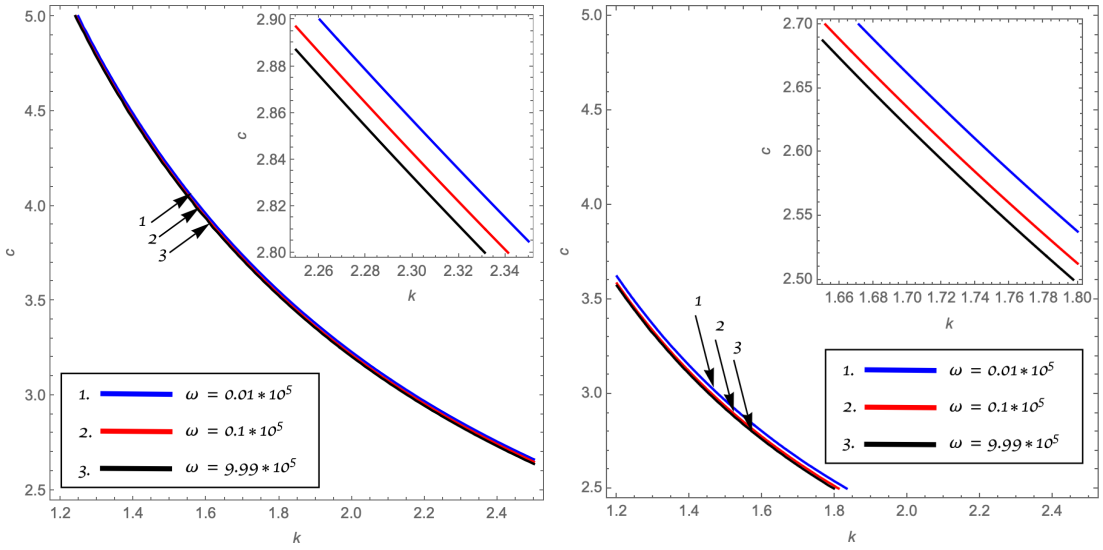


(a) (b)

Fig 6: Variation of Phase velocity (c) vs wave number (k) for the various values of HS (P_3), (a) electrically open case (EOC) (b) electrically short case (ESC).

Table 5: Comparison of hydrostatic stress P_3 on phase velocity c at $k = 1.4$

P_3	c (EOC)	Δ% (EOC)	c (ESC)	Δ% (ESC)
0.1×10^4	4.487	–	3.152	–
0.3×10^4	4.526	+0.87%	3.208	+1.78%
0.9×10^4	4.597	+2.45%	3.316	+5.20%

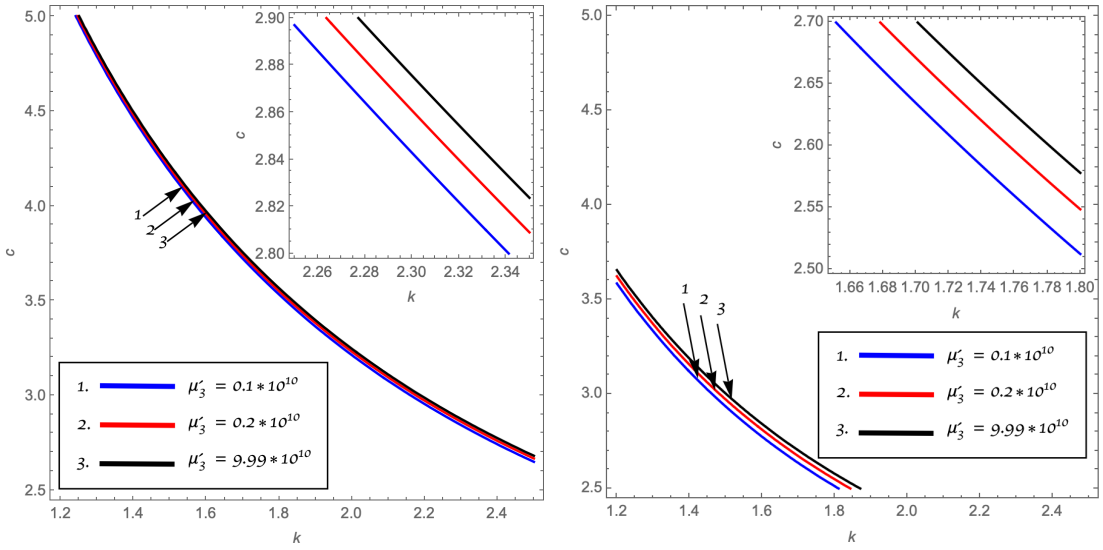


(a) (b)

Fig 7: Variation of Phase velocity (c) vs wave number (k) for the various values of the sandy parameter (ω), (a) electrically open case (EOC) (b) electrically short case (ESC).

Table 6: Comparison of sandy parameter ω on phase velocity c (read from the magnified inset panels: $k = 1.70$ for ECC, $k = 2.30$ for EOC)

ω	c (EOC)	Δ% (EOC)	c (ESC)	Δ% (ESC)
0.01×10^5	2.8568	–	2.6613	–
0.1×10^5	2.8428	-0.49%	2.6348	-1.00%
9.99×10^5	2.8326	-0.85%	2.6201	-1.55%

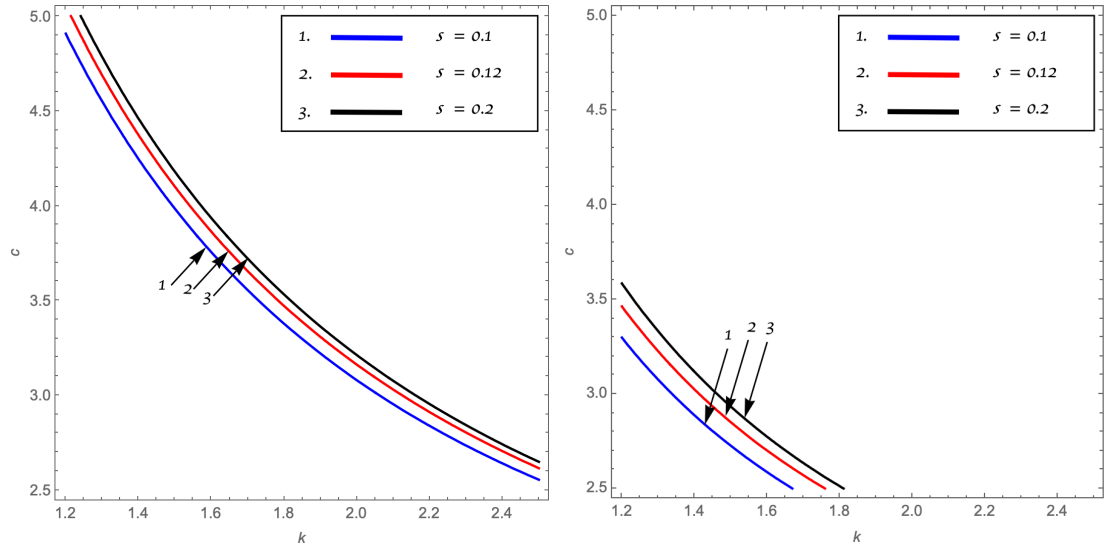


(a) (b)

Fig 8: Variation of Phase velocity (c) vs wave number (k) for the various values of internal friction (μ_3'), (a) electrically open case (EOC) (b) electrically short case (ESC).

Table 7: Comparison of internal friction μ_3' on phase velocity c (read from the magnified inset panels: $k = 1.74$ for ECC, $k = 2.30$ for EOC)

μ_3'	c (EOC)	Δ% (EOC)	c (ESC)	Δ% (ESC)
0.1×10^{10}	2.8427	–	2.5836	–
0.2×10^{10}	2.8608	+0.64%	2.6199	+1.41%
9.99×10^{10}	2.8754	+1.15%	2.6498	+2.56%

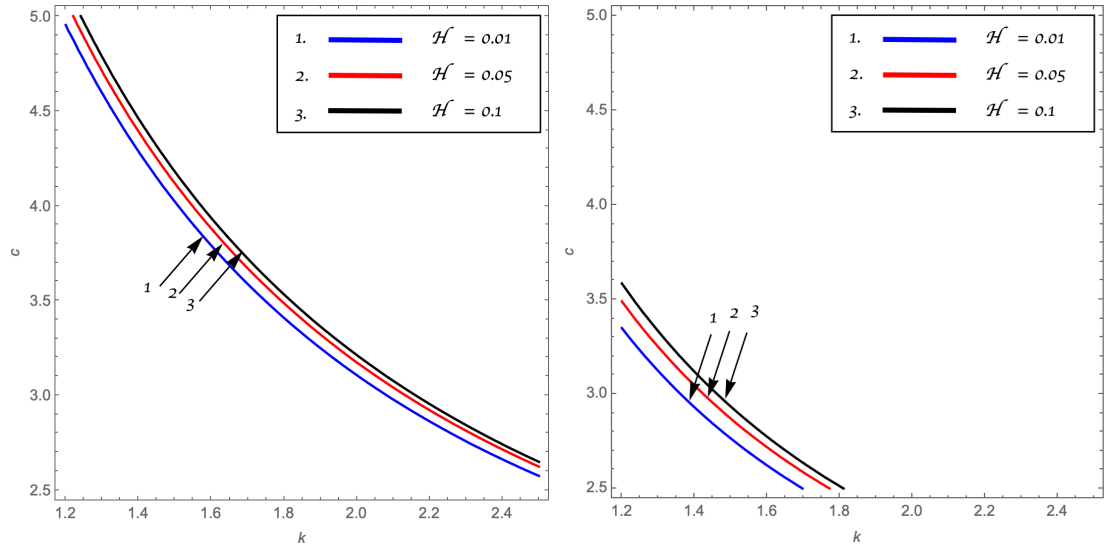


(a) (b)

Fig 9: Variation of Phase velocity (c) vs wave number (k) for the various values of irregularity span (s), (a) electrically open case (EOC) (b) electrically short case (ESC).

Table 8: Comparison of the irregularity span s on phase velocity c at $k = 1.3$

s	c (EOC)	Δ% (EOC)	c (ESC)	Δ% (ESC)
0.1	4.554	–	3.075	–
0.12	4.690	+2.99%	3.226	+4.91%
0.2	4.789	+5.16%	3.332	+8.36%



(a) (b)

Fig 10: Variation of Phase velocity (c) vs wave number (k) for the various values of irregularity depth (H), (a) electrically open case (EOC) (b) electrically short case (ESC).

Table 9: Comparison of irregularity depth H on phase velocity c at $k = 1.3$

H	c (EOC)	Δ% (EOC)	c (ESC)	Δ% (ESC)
0.01	4.597	–	3.122	–
0.05	4.711	+2.48%	3.248	+4.04%
0.1	4.789	+4.18%	3.332	+6.73%

The numerical analysis keeps the values of h_1 and h_2 fixed at 0.1 across all figures. For an electrically open circuit, Figures 2(a) to 10(a) illustrate the results obtained from equation (59) for different parameter values. Similarly, Figures 2(b) to 10(b) depict the results from equation (60) for an electrically short case (ESC) under varying parameters. In each figure, the vertical axis represents the phase velocity c, while the horizontal axis corresponds to the wave number k. The study demonstrates that phase velocity exhibits an increasing trend with a rise in wave

number for the assumed parameter values.

Figures 2(a) and 2(b) present the impact of initial stress (P_1) on the phase velocity of Love waves under electrically open and electrically short case (ESC). The dispersion curves are generated for varying values of P_1, while the initial stress (P_2) and HS (P_3) remain constant at 0.01×10^{11} and 0.01×10^4, respectively. The three curves correspond to P_1 values of $0 \times 10^6, 0.01 \times 10^6$, and 0.02×10^6. The results indicate that an increase in P_1 leads to a higher phase velocity of Love waves. Additionally, a comparison between the two cases reveals that the electrically open case (EOC)has a stronger influence than the electrically short circuit.

Figures 3(a) and 3(b) illustrate how phase velocity changes with wave number for various values of the initial stress parameter (P_2) under electrically open and electrically short case (ESC). The dispersion curves are plotted for varying values of P_2 , while the initial stress (P_1) and HS (P_3) remain fixed at 0.01×10^6 and 0.01×10^4, respectively. The values of P_2 for curves 1, 2, and 3 are set at $1 \times 10^{11}, 4 \times 10^{11}$ and 7×10^{11}, respectively. A closer examination of both figures reveals that the phase velocity of Love waves increases as P_2 increases. Furthermore, when comparing the two cases, the electrically open case (EOC)has a more dominant effect than the electrically short case (ESC).

The variation in phase velocity of Love waves with respect to the heterogeneity parameter (α) is displayed in figures 4(a) and 4(b) for electrically open case (EOC) and the electrically short case (ESC). The dispersion curves are analyzed under the conditions of an initial stress of $P_2 = 0.01 \times 10^{11}$ and a bonding parameter of $\Omega = 1$. The α values for curves 1, 2, and 3 are $0.1, 1.9$, and 4.2, respectively, with curves 1 and 2 appearing close together. The findings indicate that as α increases, the phase velocity also increases. Furthermore, the electrically open case (EOC) demonstrates stronger effects in comparison to the electrically short case (ESC).

The phase velocity of Love waves as a function of wave number and bonding parameter (Ω) is depicted in figures 5(a) and 5(b) for electrically open and short

cases. The bonding parameter is associated with the interface between the prestressed piezoelectric layer and the prestressed heterogeneous orthotropic layer. The upper and lower layer parameters are held constant at $P_1 = 0.01 \times 10^6$, $P_2 = 0.01 \times 10^{11}$, and $\alpha = 0.1$.The bonding parameter values for curves 1-3 are 1,1.00002, and 1.00008. Observations indicate that increasing Ω results in a corresponding increase in phase velocity. Additionally, the electrically open case (EOC) features closely spaced curves and demonstrates greater dominance over the electrically short case (ESC).

The dispersion characteristics of electrically open and short cases under different HS (P_3) values are depicted in figures 6(a) and 6(b). The dispersion curves are generated with fixed initial stresses, $P_1 = 0.01 \times 10^6$ and $P_2 = 0.01 \times 10^{11}$, while P_3 values for curves 1–3 are $0.1 \times 10^4, 0.3 \times 10^4$ and 0.9×10^4. Detailed observations confirm that an increase in P_3 leads to a rise in phase velocity. The electrically open case (EOC) exhibits closely packed and overlapping curves, making it more dominant than the electrically short case (ESC).

Figures 7(a) and 7(b) illustrate how phase velocity changes with wave number for different values of the sandy parameter (ω) under electrically open and short conditions. The analysis is conducted by varying ω, while keeping other parameters constant: $P_3 = 0.01 \times 10^4$,$\mu_2' = 0.1 \times 10^{10}$, $s = 0.2$,and $H = 0.2$. The selected values of ω are $0.01 \times 10^5, 0.1 \times 10^5$ and 9.99×10^5. The findings indicate that phase velocity decreases as ω increases, with a more significant effect in the electrically open case (EOC).

Figures 8(a) and 8(b) present the impact of varying internal friction (μ_2') on phase velocity as a function of wave number under electrically open and short conditions. The study is conducted by varying μ_2' while keeping HS ($P_3 = 0.01 \times 10^4$),sandy parameter ($\omega = 0.1 \times 10^5$), irregularity span ($s = 0.2$),and irregularity depth ($H = 0.2$) constant. The selected values of μ_2' for curves 1, 2, and 3 are $0.1 \times 10^{10}, 0.2 \times 10^{10}$, and 9.99×10^{10}.The results indicate that increasing μ_2' leads to a

rise in phase velocity, with the electrically open case (EOC) exerting a stronger influence and producing overlapping dispersion curves.

Figures 9(a), 10(a), 9(b), and10(b) compare phase velocity variations for different irregularity span (s) and depth (H) values under electrically open and short conditions. Other parameters, including HS ($P_3 = 0.01 \times 10^4$),sandy parameter ($\omega = 0.1 \times 10^5$) and,internal friction $\mu_2' = 0.1 \times 10^{10}$, remain unchanged. The results indicate that an increase in s and H leads to a rise in phase velocity. Additionally, the electrically open case (EOC) has a stronger effect than the electrically short circuit.

Across all the parameter sweeps, a clear sensitivity hierarchy emerges for tuning phase velocity in this layered, irregular, initially-stressed FGPM structure: the bonding parameter Ω, initial stress P_1, and heterogeneity parameter α exert the strongest control (up to 15%, 15%, and 8.5% shift in c under ESC, respectively), the irregularity parameters H and s and initial stress P_3 offer moderate, near-linear tunability ($4-7\%$), while P_2, internal friction μ_3', and the sandy parameter ω produce only marginal, sub-3% changes. For SAW filter and resonator design, this ranking is directly actionable: Ω, P_1, and α are the natural coarse-tuning knobs for setting a device's center frequency and bandwidth, since even modest adjustments produce strong dispersion shifts, while H,s, and P_3 suit fine-tuning of the passband, and P_2, μ_3' , and ω can be treated as robust, low-sensitivity degrees of freedom whose fabrication tolerances are unlikely to significantly detune a SAW device. Notably, the ESC condition consistently shows a larger percentage sensitivity than the electrically open-circuit (EOC) condition for every single parameter tested, indicating that ESC operation offers superior electromechanical coupling and tunability making it the preferable configuration for actively tunable SAW filters whereas the comparatively stable EOC response is better suited to applications requiring a drift-resistant reference frequency, such as precision SAW

oscillators.

The results of our study provide critical insights into the potential application of this heterogeneous prestressed orthotropic structure in surface acoustic wave (SAW) devices. The observed increase in phase velocity with parameters such as initial stress, HS, heterogeneity, and bonding suggests that this material configuration enhances wave propagation efficiency, which is essential for high-frequency SAW devices. The dominance of electrically open conditions over short conditions indicates a strong electromechanical coupling effect, which is advantageous for signal processing applications. Additionally, the sensitivity of phase velocity to sandy parameter variations implies that the material can be tailored for sensor applications, particularly in detecting environmental changes or mechanical perturbations. However, the reduction in phase velocity due to increasing sandy parameters highlights the need for precise material engineering to minimize wave attenuation. Overall, this study confirms that the proposed material configuration can improve the performance of SAW devices by enhancing wave velocity, sensitivity, and electromechanical interaction, making it highly suitable for advanced sensing, signal filtering, and communication technologies.

11 Conclusion

The present study investigates the propagation of Love-type waves in a heterogeneous pre-stressed orthotropic layer bonded between a pre-stressed piezoelectric layer and an IVS substrate subjected to HS. For electrically open case (EOC) and electrically short case (ESC), dispersion relation is derived, and numerical analysis highlights the influence of key parameters such as HS, loosely bonded interface, initial stress, material heterogeneity, and irregular surface characteristics on phase velocity. The findings indicate that an increase in initial stress, heterogeneity parameter, HS, and bonding parameter enhances the Love waves phase

velocity, whereas a higher sandy parameter results in a decrease in wave speed. The dominance of electrically open cases (EOC) over electrically short case (ESC) underscores the significant role of electromechanical coupling in the studied structure. The results demonstrate the practical applicability of the proposed model in the development of surface acoustic wave (SAW) devices, offering insights for optimizing wave propagation efficiency in high-frequency sensing and communication technologies.

- Phase velocity increases with HS, initial stress, heterogeneity, and bonding parameters.
- Electrically open circuits exhibit stronger electromechanical effects than short circuits.
- Higher sandy parameters result in a decrease in phase velocity, highlighting the need for precise material engineering.
- The proposed structure shows potential for enhancing SAW device performance, particularly in signal filtering, sensing, and communication.
- These findings can guide material engineering for next-generation SAW-based sensors and RF components.
- This research provides a strong foundation for further studies aimed at refining SAW device efficiency and exploring new engineering applications in wave propagation.
- Investigating the impact of temperature variations and thermal stresses on wave propagation.
- Exploring the influence of different irregularity profiles beyond the parabolic type for broader geophysical applications.

12 Appendix

$$P_{11} = Q_{11} = \left(e_{44}^{(p)} + \frac{\left(g_{15}^{(p)}\right)^2}{\kappa_{11}^{(p)}} \right) kn\ e^{knh_0},$$

$$P_{12} = Q_{12} = -\left(e_{44}^{(p)} + \frac{\left(g_{15}^{(p)}\right)^2}{\kappa_{11}^{(p)}} \right) kne^{-knh_0}, P_{13} = Q_{13} = g_{15}^{(p)} ke^{kh_0},$$

$$P_{14} = Q_{14} = -g_{15}^{(p)} ke^{-kh_0}, \quad P_{15} = Q_{15} = 0, \quad P_{16} = Q_{16} = 0, \quad P_{17} = Q_{17} = 0,$$

$$P_{21} = Q_{21} = \frac{g_{15}^{(p)}}{\kappa_{11}^{(p)}} e^{knh_0}, \quad P_{22} = Q_{22} = \frac{g_{15}^{(p)}}{\kappa_{11}^{(p)}} e^{-knh_0}, \quad P_{23} = Q_{23} = e^{kh_0},$$

$$P_{24} = Q_{24} = e^{-kh_0}, \quad P_{25} = Q_{25} = 0, \quad P_{26} = Q_{26} = 0, \quad P_{27} = Q_{27} = 0$$

$$Q_{21} = 0, \quad Q_{22} = 0, \quad Q_{23} = \kappa_{11}^{(p)} ke^{kh_0}, \quad Q_{24} = -\kappa_{11}^{(p)} ke^{-kh_0},$$

$$Q_{25} = 0, \quad Q_{26} = 0, \quad Q_{27} = 0$$

$$P_{31} = Q_{31} = \left(e_{44}^{(p)} + \frac{\left(g_{15}^{(p)}\right)^2}{\kappa_{11}^{(p)}} \right) kne^{-knh_2}, P_{32} = Q_{32} = -\left(e_{44}^{(p)} + \frac{\left(g_{15}^{(p)}\right)^2}{\kappa_{11}^{(p)}} \right) kne^{knh_2},$$

$$P_{33} = Q_{33} = g_{15}^{(p)} ke^{-kh_2}, P_{34} = Q_{34} = g_{15}^{(p)} ke^{kh_2},$$

$$P_{35} = Q_{35} = -\left(\frac{\delta \cos(\delta h_2)}{\sqrt{1-\sin(\alpha h_2)}} + \frac{\alpha \sin(\delta h_2)\cos(\alpha h_2)}{2(1-\sin(\alpha h_2))^{3/2}} \right) M_2(1-\sin(\alpha h_2)),$$

$$P_{36} = Q_{36} = \left(-\frac{\alpha \cos(\delta h_2)\cos(\alpha h_2)}{2(1-\sin(\alpha h_2))^{3/2}} + \frac{\delta \sin(\delta h_2)}{\sqrt{1-\sin(\alpha h_2)}} \right) M_2(1-\sin(\alpha h_2)),$$

$$P_{37} = Q_{37} = 0,$$

$$P_{41} = Q_{41} = \frac{g_{15}^{(p)}}{\kappa_{11}^{(p)}} e^{-knh_2}, \quad P_{42} = Q_{42} = \frac{g_{15}^{(p)}}{\kappa_{11}^{(p)}} e^{knh_2}, \quad P_{43} = Q_{43} = e^{-kh_2}, \quad P_{44} = Q_{44} = e^{kh_2},$$

$$P_{45} = Q_{45} = 0, \quad P_{46} = Q_{46} = 0, \quad P_{47} = P_{47} = 0,$$

$$P_{51} = Q_{51} = \left((1-\Omega) \left(e_{44}^{(p)} + \frac{\left(g_{15}^{(p)}\right)^2}{\kappa_{11}^{(p)}} \right) kn - ikN\Omega \frac{c}{\beta_1} \right) e^{-knh_2},$$

$$P_{52} = Q_{52} = \left((1-\Omega) \left(e_{44}^{(p)} + \frac{\left(g_{15}^{(p)}\right)^2}{\kappa_{11}^{(p)}} \right) kn + ikN\Omega \frac{c}{\beta_1} \right) e^{knh_2},$$

$$P_{53} = P_{53} = (1-\Omega) g_{15}^{(p)} k e^{-kh_2}, \quad P_{54} = P_{54} = -(1-\Omega) g_{15}^{(p)} k e^{kh_2},$$

$$P_{55} = P_{55} = -ikN\Omega \frac{c}{\beta_1} \left(\frac{-\sin(\delta h_2)}{\sqrt{1-\sin(\alpha h_2)}} \right),$$

$$P_{56} = P_{56} = -ikN\Omega \frac{c}{\beta_1} \left(\frac{\cos(\delta h_2)}{\sqrt{1-\sin(\alpha h_2)}} \right), \quad P_{57} = P_{57} = 0,$$

$$P_{61} = Q_{61} = 0, \quad P_{62} = Q_{62} = 0, \quad P_{63} = Q_{63} = 0, \quad P_{64} = Q_{64} = 0,$$

$$P_{65} = Q_{65} = \frac{\sin(\delta\varepsilon_1 h(x))}{\sqrt{1+\sin(\alpha\varepsilon_1 h(x))}}, \quad P_{66} = Q_{66} = \frac{\cos(\delta\varepsilon_1 h(x))}{\sqrt{1+\sin(\alpha\varepsilon_1 h(x))}}, \quad P_{67} = Q_{67} = e^{-m\varepsilon_1 h(x)}$$

$$P_{71} = Q_{71} = 0, \quad P_{72} = Q_{72} = 0, \quad P_{73} = Q_{73} = 0, \quad P_{74} = Q_{74} = 0,$$

$$P_{75} = Q_{75} = M_2\delta \cos(\delta\varepsilon_1 h(x)) \sqrt{1+\sin(\alpha\varepsilon_1 h(x))} - \frac{M_2\alpha \sin(\delta\varepsilon_1 h(x)) \cos(\alpha\varepsilon_1 h(x))}{2\sqrt{1+\sin(\alpha\varepsilon_1 h(x)))}},$$

$$P_{76} = Q_{76} = -M_2\delta \sin(\delta\varepsilon_1 h(x)) \sqrt{1+\sin(\alpha\varepsilon_1 h(x))} - \frac{M_2\alpha \cos(\delta\varepsilon_1 h(x)) \cos(\alpha\varepsilon_1 h(x))}{2\sqrt{1+\sin(\alpha\varepsilon_1 h(x)))}},$$

$$P_{77} = Q_{77} = -me^{-m\varepsilon_1 h(x)}(\mu_3 - i\mu_3' kc)$$

Funding declaration:

"The authors declare that no funds, grants, or other support were received during the preparation of this manuscript."

Data availability:

All data generated or analysed during this study are included in the published article. The material parameters used in this study are adopted from previously published works such as [22], [23] and [24].

References

[1] B. Jakoby, M.J. Vellekoop, Smart Mater. Struct. 6, 668 (1997) https://doi.org/10.1088/0964-1726/6/6/003

[2] J. Du, G.L. Harding, J.A. Ogilvy, P.R. Dencher, M. Lake, Sensors Actuators A: Phys. 56, 211 (1996) https://doi.org/10.1016/S0924-4247(96)01311-8

[3] J. Liu, S. He, Int. J. Solids Struct. 47, 169 (2010) https://doi.org/10.1016/j.ijsolstr.2009.06.018

[4] S.A. Sahu, A. Singhal, S. Chaudhary, J. Intell. Mater. Syst. Struct. 29, 423 (2018) https://doi.org/10.1177/1045389X17708047

[5] P.K. Saroj, S.A. Sahu, S.Chaudhary, A. Chattopadhyay, Waves Random Complex Media 25, 608 (2015) https://doi.org/10.1080/17455030.2015.1063738

[6] S.V. Biryukov, Y.V. Gulyaev, V.V. Krylov, V.P. Plessky, Surface acoustic waves in inhomogeneous media (Springer, 1995) https://doi.org/10.1007/978-3-642-57767-3

[7] X.Y. Li, Z.K. Wang, S.H. Huang, Int. J. Solids Struct. 41, 7309 (2004) https://doi.org/10.1016/j.ijsolstr.2004.05.064

[8] G.R. Liu, K.Y. Dai, X. Han, T. Ohyoshi, J. Sound Vib. 268, 131 (2003) https://doi.org/10.1016/S0022-460X(02)01494-3

[9] G.R. Liu, J. Tani, Surface waves in functionally gradient piezoelectric plates (1994) https://doi.org/10.1115/1.2930447

[10] P. Alam, S. Kundu, S. Gupta, A. Saha, Waves Random Complex Media 28, 182 (2018) https://doi.org/10.1080/17455030.2017.1335915

[11] A.K. Singh, K.C. Mistri, A. Das, Waves Random Complex Media 27, 213 (2017) https://doi.org/10.1080/17455030.2016.1213461

[12] S. Dey, A.K. Gupta, S. Gupta, J. Eng. Mech. 128, 1115 (2002) https://doi.org/10.1061/(ASCE)0733-9399(2002)128:10(1116)

[13] S.K. Tomar, J. Kaur, Acta Mech. 190, 1 (2007) https://doi.org/10.1007/s00707-006-0423-7

[14] A. Ray, A.K. Singh, Acta Mech. 231, 101 (2020) https://doi.org/10.1007/s00707-019-02525-5

[15] A. Chattopadhyay, S. Gupta, S.A. Sahu, A.K. Singh, J. Vib. Control 19, 109 (2013) https://doi.org/10.1177/1077546311430699

[16] A.K. Singh, S. Kumar, A. Chattopadhyay, Int. J. Eng. Sci. 89, 35 (2015) https://doi.org/10.1016/j.ijengsci.2014.11.008

[17] J. Du, X. Jin, J. Wang, Acta Mech. 192, 169 (2007) https://doi.org/10.1007/s00707-006-0435-3

[18] P. Singh, A.Chattopadhyay, A.K. Singh, Waves Random Complex Media 31, 942 (2021) https://doi.org/10.1080/17455030.2019.1635291

[19] G. Murty, Phys. Earth Planet. Inter. 11, 65 (1975) https://doi.org/10.1016/0031-9201(75)90076-X

[20] G.S. Murty, Geophys. J. Int. 44, 389 (1976) https://doi.org/10.1111/j.1365-246X.1976.tb03663.x

[21] Z. Wang, F. Shang, Acta Mech. Solida Sin. 18, 101 (1997)

[22] A. Singhal, R. Tiwari, J. Baroi, R. Kumhar, Waves Random Complex Media, 1 (2022) https://doi.org/10.1080/17455030.2022.2026522

[23] B. Prasad, S. Kundu, P.C. Pal, P. Alam, Arabian J. Geosci. 13, 1 (2020) https://doi.org/10.1007/s12517-020-05354-2

[24] A.K. Singh, K.C. Mistri, A. Das, Waves Random Complex Media 27, 213 (2017) https://doi.org/10.1080/17455030.2016.1213461

Supplementary Files

This is a list of supplementary files associated with this preprint. Click to download.

- A4supplementarymaterial.pdf